

## Article

# 1,4-Bis((9H-Carbazol-9-yl)Methyl)Benzene-Containing Electrochromic Polymers as Potential Electrodes for High-Contrast Electrochromic Devices

Chung-Wen Kuo<sup>1</sup>, Jui-Cheng Chang<sup>2,3</sup>, Li-Ting Lee<sup>4</sup>, Yi-Dong Lin<sup>1</sup>, Pei-Ying Lee<sup>2</sup> and Tzi-Yi Wu<sup>2,\*</sup>

<sup>1</sup> Department of Chemical and Materials Engineering, National Kaohsiung University of Science and Technology, Kaohsiung 80778, Taiwan; welly@nkust.edu.tw (C.-W.K.); a5202350@gmail.com (Y.-D.L.)

<sup>2</sup> Department of Chemical Engineering and Materials Engineering, National Yunlin University of Science and Technology, Yunlin 64002, Taiwan; d700215@gmail.com (J.-C.C.); leepeiying1018@gmail.com (P.-Y.L.)

<sup>3</sup> Bachelor Program in Interdisciplinary Studies, National Yunlin University of Science and Technology, Yunlin 64002, Taiwan

<sup>4</sup> Department of Materials Science and Engineering, Feng Chia University, Taichung 40724, Taiwan; ltleefcu.edu.tw

\* Correspondence: wuty@gmail.yuntech.edu.tw; Tel.: +886-5-534-2601 (ext. 4626)

**Abstract:** Four 1,4-bis((9H-carbazol-9-yl)methyl)benzene-containing polymers (PbCmB, P(bCmB-co-bTP), P(bCmB-co-dbBT), and P(bCmB-co-TF)) were electrosynthesized onto ITO transparent conductive glass and their spectral and electrochromic switching performances were characterized. The PbCmB film displayed four types of color variations (bright gray, dark gray, dark khaki, and dark olive green) from 0.0 to 1.2 V. P(bCmB-co-bTP) displayed a high transmittance variation ( $\Delta T = 39.56\%$  at 685 nm) and a satisfactory coloration efficiency ( $\eta = 160.5 \text{ cm}^2 \cdot \text{C}^{-1}$  at 685 nm). Dual-layer organic electrochromic devices (ECDs) were built using four bCmB-containing polycarbazoles and poly(3,4-ethylenedioxythiophene) (PEDOT) as anodes and a cathode, respectively. PbCmB/PEDOT ECD displayed gainsboro, dark gray, and bright slate gray colors at  $-0.4 \text{ V}$ ,  $1.0 \text{ V}$ , and  $2.0 \text{ V}$ , respectively. The P(bCmB-co-bTP)/PEDOT ECD showed a high  $\Delta T$  (40.7% at 635 nm) and a high coloration efficiency ( $\eta = 428.4 \text{ cm}^2 \cdot \text{C}^{-1}$  at 635 nm). The polycarbazole/PEDOT ECDs exhibited moderate open circuit memories and electrochemical redox stability. The characterized electrochromic properties depicted that the as-prepared polycarbazoles had a satisfactory application prospect as an electrode for the ECDs.

**Keywords:** electrosynthesis; redox process; color-bleach kinetics; electrochromic device; electrochemical redox stability



**Citation:** Kuo, C.-W.; Chang, J.-C.; Lee, L.-T.; Lin, Y.-D.; Lee, P.-Y.; Wu, T.-Y. 1,4-Bis((9H-Carbazol-9-yl)Methyl)Benzene-Containing Electrochromic Polymers as Potential Electrodes for High-Contrast Electrochromic Devices. *Polymers* **2022**, *14*, 1175. <https://doi.org/10.3390/polym14061175>

Academic Editor: Mohammad Afsar Uddin

Received: 16 February 2022

Accepted: 11 March 2022

Published: 15 March 2022

**Publisher's Note:** MDPI stays neutral with regard to jurisdictional claims in published maps and institutional affiliations.



**Copyright:** © 2022 by the authors. Licensee MDPI, Basel, Switzerland. This article is an open access article distributed under the terms and conditions of the Creative Commons Attribution (CC BY) license (<https://creativecommons.org/licenses/by/4.0/>).

## 1. Introduction

Electrochromism refers to a phenomenon exhibited by certain electroactive species with reversible changes of color and absorption spectra in response to an applied voltage. Many classes of compounds and materials have been shown to exhibit electrochromism over the past four decades. Inorganic transition metal oxides (e.g.,  $\text{WO}_3$ ,  $\text{TiO}_2$ ,  $\text{V}_2\text{O}_5$ , and  $\text{NiO}$ ), inorganic coordination complexes (e.g., Prussian blue),  $\pi$ -conjugated polymers, and molecular dyes are the most frequently studied electrochromic materials [1–5].  $\pi$ -conjugated polymers have recently attracted an increasing interest due to their superior benefits such as their ease of solution processing, rapid switching speeds, high coloration efficiency, and rich color palette during usage for electrochromic devices.  $\pi$ -conjugated polymers have a wide range of optical and electrochemical applications in field-effect transistors [6,7], capacitors [8,9], photovoltaic cells [10,11], light-emitting diodes [12,13], catalyst supports [14,15], and sensors [16,17].

Nowadays, the most popular  $\pi$ -conjugated polymers (e.g., polythiophenes [18], polyaniline [19,20], polyindoles [21], polycarbazole [22,23], polyfurans [24], polypyrenes [25],

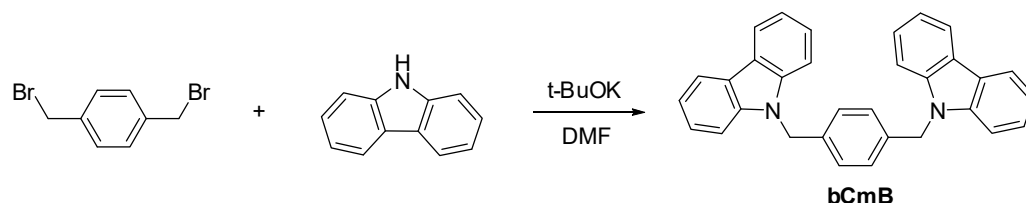
and PEDOT-PSS [26]) are widely applied to organic electrochromic devices. Among the many promising  $\pi$ -conjugated polymers, carbazole-containing polymers have attractive optoelectronic properties due to their hole-transporting characteristics via the radical cation and dication species as well as their ease of oxidation through the nitrogen centers. Moreover, polycarbazoles can easily be functionalized at the *N*-, 3,6-, and 2,7-positions, which brings further benefits to modify the electrochromic properties of the resulting polymers. For instance, Ak et al. reported the electrochromic performances of a disulfide-linked polycarbazole (PCS). The PCS was electrosynthesized in BFEE-containing and BFEE-free electrolytic solutions. The PCS prepared in the BFEE-containing electrolytic solution had a high optical contrast (62.5%) and a low response time of 2.0 s [27]. Niu et al. synthesized a series of phenylcarbazole-containing polyimides (PI-6A, PI-6B, PI-6C, PI-6D, and PI-6E). The PI-6A film changed from light yellow (0.0 V), to brown yellow (0.8 V), to deep yellow (1.1 V). The  $\Delta T$  and coloration efficiency of PI-6D were 57% and  $250 \text{ cm}^2 \cdot \text{C}^{-1}$ , respectively, at 568 nm. In addition, five polyimides had a high retained electroactivity ( $\geq 88\%$ ) after 600 cycles [28]. Poly(3,4-ethylenedioxythiophene) (PEDOT) is a derivative of polythiophenes. PEDOT displays a satisfactory electrochemical reversibility and a high transmittance modulation between its oxidized and neutral states [29]. PEDOT is transparent or dark blue in its oxidized or neutral states, respectively. Accordingly, PEDOT is a potential cathodically coloring layer. Another method is copolymerization (or blending), which is a facile technique for tuning the electrochromic properties of conjugated polymers. The monomers used in copolymerization are bithiophene, 3,3'-dibromo-2,2'-bithiophene, and 2-(thiophen-2-yl)furan. The conjugated length of 2,2'-bithiophene is larger than that of a single thiophene ring; the  $E_{\text{onset}}$  of 2,2'-bithiophene is smaller than that of a single thiophene ring [30]. 3,3'-dibromo-2,2'-bithiophene comprises two additional bromide substituents in the 2,2'-bithiophene unit. Electron-withdrawing bromide substituents increase the  $E_{\text{onset}}$  of the polymers. 2-(thiophen-2-yl)furan contains the optical and electrochemical properties of thiophene and furan; the conjugated polymer chain length of 2-(thiophen-2-yl)furan is greater than those of thiophene and furan.

The use of polymonocarbazole derivatives in electrochromic applications is limited due to their low transmittance change and poor film-forming characteristics. Recently, conjugated polymers with a high transmittance change and good film-forming quality have been achieved by electropolymerizing two or more carbazole-containing monomers [31]. In this present work, a biscarbazole-containing derivative (bCmB) was synthesized and its corresponding homopolymer (PbCmB) and copolymers (P(bCmB-co-bTP), P(bCmB-co-dbBT), and P(bCmB-co-TF)) were electrocoated onto ITO glass substrates. Two carbazole groups of a bCmB unit were bridged by a phenyl and two methylene groups. The incorporation of the methylene groups into the bCmB unit increased the solubility of the resulting polymer. The electrochemical properties, UV-Vis spectra, and switching kinetics of the anodic polymers were characterized. In addition, four dual-layer organic ECDs were built using PbCmB, P(bCmB-co-bTP), P(bCmB-co-dbBT), and P(bCmB-co-TF) as the anodes and PEDOT as the cathode. The UV-Vis spectra, color transitions, switching time, and long-term redox cycling stability of the four ECDs were comprehensively explored.

## 2. Experiment

### 2.1. Materials

Carbazole, 1,4-bis(bromomethyl)benzene, potassium *tert*-butoxide, and EDOT were purchased from Aldrich, Alfa Aesar, and the Tokyo Chemical Industry, respectively. Dimethyl formamide (DMF) was dried with  $4 \text{ \AA}$  molecular sieves prior to use. The synthetic scheme of bCmB is displayed in Figure 1. The gel electrolyte between the anode and the cathode of the ECDs was prepared using PMMA,  $\text{LiClO}_4$ , and PC according to previous procedures [26]. Poly(methyl methacrylate) (PMMA) ( $M_w = 350,000$ ; Acros Organics),  $\text{LiClO}_4$ , and propylene carbonate (PC) ( $M_w = 120$ ; Alfa Aesar) were also commercially available and used as received.



**Figure 1.** Synthesis of bCmB.

## 2.2. Synthesis of 1,4-Bis((9H-carbazol-9-yl)methyl)benzene (bCmB)

A mixture of carbazole (5.35 g, 32 mmol), 1,4-bis(bromomethyl)benzene (3.96 g, 15 mmol), and 20 mL of DMF was added to a 100 mL two-necked glass reactor. The solution was cooled to 0 °C, treated with potassium *tert*-butoxide (4.26 g, 38 mmol), and then refluxed for 24 h. The quantity of each portion was 7.6 mmol. After cooling, the DMF solvent was evaporated at a reduced pressure (33 mmHg) and an elevated temperature (145 °C) and the remaining mixture was extracted with a 200 mL H<sub>2</sub>O/200 mL CH<sub>2</sub>Cl<sub>2</sub> mixture. The organic phase (CH<sub>2</sub>Cl<sub>2</sub> layer) was cleaned with 200 mL brine, further cleaned with 200 mL H<sub>2</sub>O, and then dried using MgSO<sub>4</sub> for half an hour. The crude product was further purified by column chromatography (silica gels, DCM/*n*-hexane = 1/2 as an eluent). The mass and yield of the reaction product were 5.04 g and 77%, respectively. The <sup>1</sup>H NMR (500 MHz, CDCl<sub>3</sub>) results were: δ = 5.44 (s, 4H, -NCH<sub>2</sub>); 7.01 (s, 4H, benzene-H); 7.22 (t, J = 7.6 Hz, 4H, carbazole-H); 7.30 (d, J = 7.6 Hz, 4H, carbazole-H); 7.39 (t, J = 7.6 Hz, 4H, carbazole-H); and 8.10 (d, J = 7.6 Hz, 4H, carbazole-H). The <sup>13</sup>C NMR (175 MHz, DMSO-*d*<sub>6</sub>) results were δ = 46.1, 108.8, 119.2, 120.4, 123.0, 125.8, 126.8, 136.5, and 140.5. The elemental analysis calculated (elem. anal. calc.) for C<sub>32</sub>H<sub>24</sub>N<sub>2</sub> was: C, 88.04%; H, 5.54%; and N, 6.42% with C, 87.92%; H, 5.50%; and N, 6.31% found.

## 2.3. Electrodepositions of PbCmB, PEDOT, P(bCmB-co-bTP), P(bCmB-co-dbBT), and P(bCmB-co-TF) Electrodes

PbCmB, PEDOT, P(bCmB-co-bTP), P(bCmB-co-dbBT), and P(bCmB-co-TF) electrodes were potentiostatically electrodeposited at 1.0 V (vs. Ag/AgNO<sub>3</sub>) on an ITO glass substrate with a charge density of 20 mC·cm<sup>-2</sup>. The concentration of bCmB, bTP, dbBT, and TF monomers was 2 × 10<sup>-3</sup> M and the liquid electrolyte was 0.2 M LiClO<sub>4</sub> in ACN/DCM (1:1 by volume). The feed species and concentrations of the monomers are shown in Table 1. The reference and counter electrodes of the liquid electrolyte cell were an Ag/AgNO<sub>3</sub> electrode (calibrated with ferrocene/ferrocenium) and a Pt wire, respectively. The polymeric electrode area was 1.5 cm<sup>2</sup>.

**Table 1.** Feed species of polymeric electrodes.

Electrodes	Anodic Polymers	Feed Species of Anodic Polymer	Feed Molar Ratio of Anodic Polymer
(a)	PbCmB	2 mM bCmB	Neat bCmB
(b)	P(bCmB-co-bTP)	2 mM bCmB + 2 mM bTP	2:2
(c)	P(bCmB-co-dbBT)	2 mM bCmB + 2 mM dbBT	2:2
(d)	P(bCmB-co-TF)	2 mM bCmB + 2 mM TF	2:2

## 2.4. Fabrication of the Dual-Layer ECDs

The PMMA/LiClO<sub>4</sub>/PC composite electrolyte was coated onto PbCmB, P(bCmB-co-bTP), P(bCmB-co-dbBT), and P(bCmB-co-TF) anodically coloring films. The cathodically coloring film (PEDOT) was placed onto the PMMA/LiClO<sub>4</sub>/PC layer. The sandwich configuration of the ECDs was anodically coloring film/electrolyte/cathodically coloring film. The active areas of PbCmB, P(bCmB-co-bTP), P(bCmB-co-dbBT), P(bCmB-co-TF), and PEDOT were ca. 1.0 × 1.5 cm<sup>2</sup>.

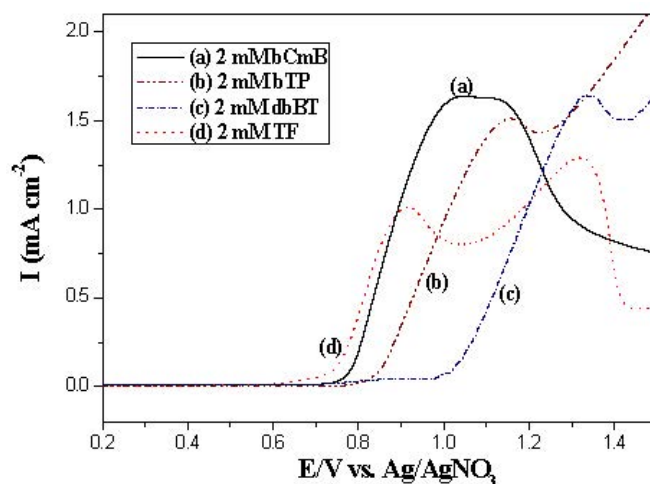
### 2.5. Electrochemical, Electrochromic, and Kinetic Characterizations

The electrochemical polymerization procedures and electrochemical properties of the PbCmB, P(bCmB-co-bTP), P(bCmB-co-dbBT), and P(bCmB-co-TF) anodically coloring films were carried out using a CHI6277E (CH Instruments, Austin, TX, USA) electrochemical workstation with a scan rate of  $100 \text{ mV s}^{-1}$ . The absorption spectra and electrochromic switching performances of the single-layer electrodes in the solutions and the dual-layer ECDs were measured using a spectrophotometer (Jasco V-630 (JASCO International Co., Ltd., Tokyo, Japan)) and an electrochemical workstation (CHI6277E). The color-bleach kinetics of the polymers were switched between 0.0 and 1.2 V whereas the color-bleach kinetics of the ECDs were switched between  $-0.4 \text{ V}$  and 1.8 V.

## 3. Results and Discussion

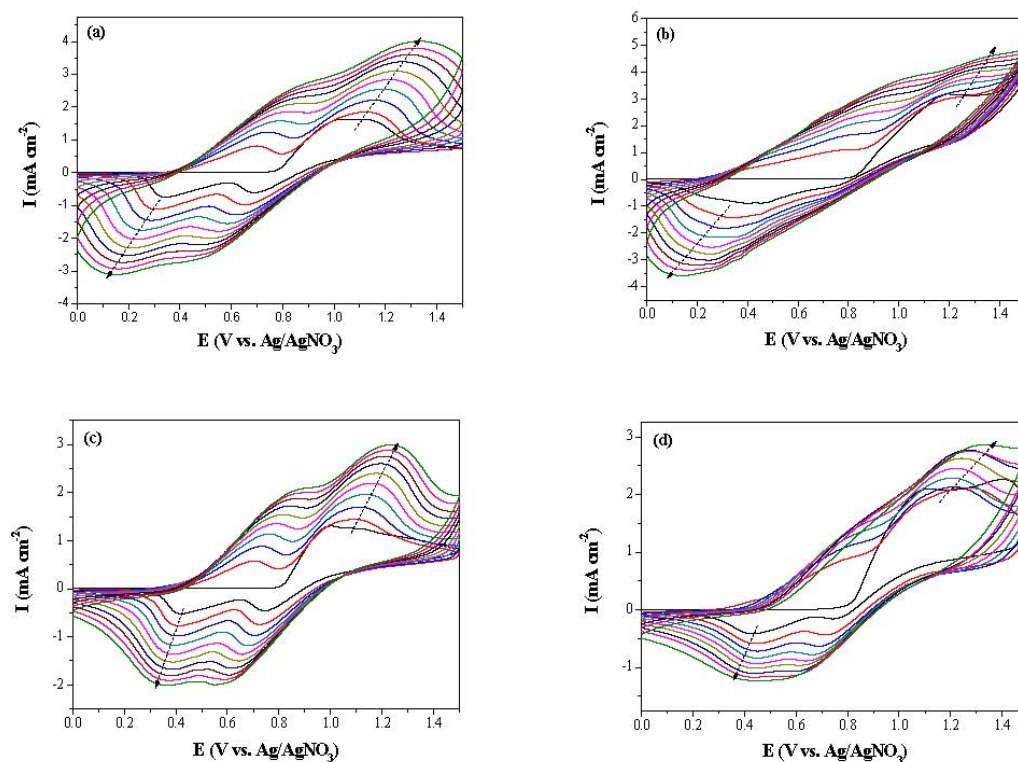
### 3.1. Electrochemical Characterization of the Polymer Electrodes

Figure 2 shows the linear sweep voltammetry curves for the electrochemical oxidation of neat PbCmB, P(bCmB-co-bTP), P(bCmB-co-dbBT), and P(bCmB-co-TF) in a  $0.2 \text{ M LiClO}_4$  solution. The onset potentials in the cyclic voltammetry of neat bCmB, bTP, dbBT, and TF were 0.75, 0.81, 0.94, and 0.70 V (vs. Ag/AgNO<sub>3</sub>), respectively. The incorporation of two electron-withdrawing bromide groups in the bithiophene unit increased the onset potentials. bCmB displayed a lower onset potential than the bithiophene unit; this could be attributed to the fact that biscarbazole-containing bCmB showed a stronger electron-donating ability than the bithiophene unit. The disparities of the onset potentials between neat bCmB and neat bithiophene derivatives were less than 0.2 V, implying the feasibility of copolymerizations using bCmB and bithiophene derivatives.



**Figure 2.** Cyclic voltammograms of (a) 2 mM bCmB, (b) 2 mM bTP, (c) 2 mM dbBT, and (d) 2 mM TF containing  $0.2 \text{ M LiClO}_4$  at a scan rate of  $100 \text{ mV s}^{-1}$ .

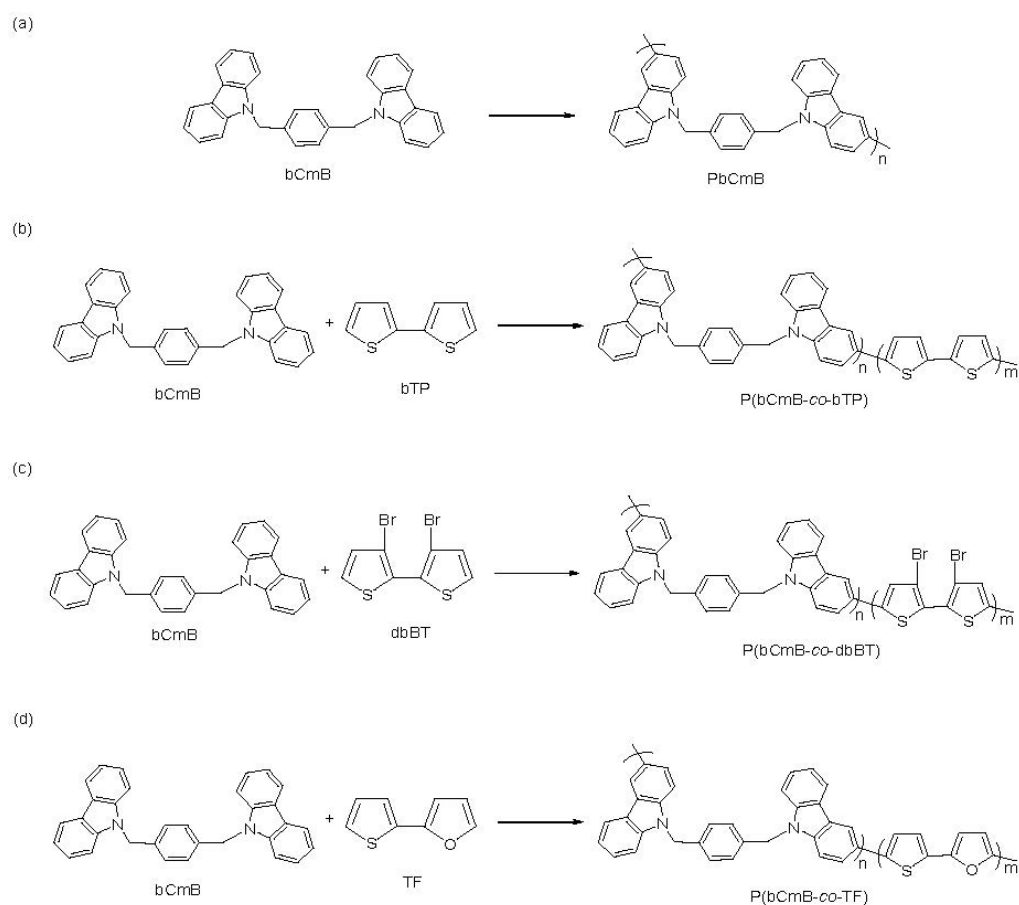
Figure 3 displays the electrogrowth of neat bCmB and mixtures of bCmB + bithiophene derivatives (or 2-(thiophen-2-yl)furan) in  $0.2 \text{ M LiClO}_4/\text{ACN}/\text{DCM}$ . The potentiodynamic polymerization scans from the first to the tenth cycles revealed that the current densities of the redox peaks increased with the number of increasing cycles, implying the growth of polymers on the ITO substrate [32]. As shown in Figure 3a, PbCmB displayed two distinct oxidation peaks at 0.70 and 1.12 V as well as two evident reduction peaks at 0.31 and 0.65 V.



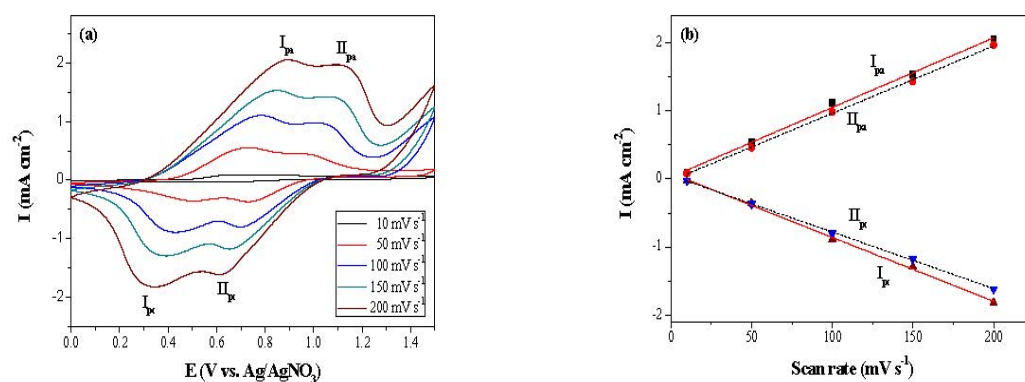
**Figure 3.** Electrochemical synthesis of (a) PbCmB, (b) P(bCmB-co-bTP), (c) P(bCmB-co-dbBT), and (d) P(bCmB-co-TF) in an ACN/DCM (1:1 by volume) solution at  $100 \text{ mV s}^{-1}$  on ITO glass.

The first oxidation and reduction peaks depicted the generation of radical cations in poly(1,4-bis((9H-carbazol-9-yl)methyl)benzene) and the second redox peaks represented the formation of dications. The incorporation of bithiophene, 3,3'-dibromo-2,2'-bithiophene, and 2-(thiophen-2-yl)furan into the polymeric chain slightly shifted the redox peaks. The first oxidation and reduction peaks of P(bCmB-co-bTP) were located at 0.78 and 0.33 V, respectively (Figure 3b). In a similar condition, two oxidation peaks of P(bCmB-co-dbBT) were situated at 0.70 and 1.09 V, respectively, and two reduction peaks of P(bCmB-co-dbBT) were located at 0.41 and 0.72 V, respectively (Figure 3c). The first and second oxidation peaks of P(bCmB-co-TF) were located at 0.79 and 1.26 V, respectively, and the first and second reduction peaks of P(bCmB-co-TF) were situated at 0.44 and 0.71 V, respectively (Figure 3d). The peak potentials and CV wave shapes of PbCmB were diverse compared with those of P(bCmB-co-bTP), P(bCmB-co-dbBT), and P(bCmB-co-TF), proving the coating of P(bCmB-co-bTP), P(bCmB-co-dbBT), and P(bCmB-co-TF) membranes onto the ITO glass substrate. The polymerization schemes of PbCmB, P(bCmB-co-bTP), P(bCmB-co-dbBT), and P(bCmB-co-TF) are listed in Figure 4 [33].

The electrocoated P(bCmB-co-bTP) film was studied using various scan rate cyclic voltammetry measurements. As displayed in Figure 5, the P(bCmB-co-bTP) film showed two couples of well-defined redox peaks at various scan rates in 0.2 M LiClO<sub>4</sub>/ACN/DCM; the peak current densities of the P(bCmB-co-bTP) film were linearly proportional to the scan velocities, representing that P(bCmB-co-bTP) tightly adhered to the conductive glass and the redox behaviors of P(bCmB-co-bTP) were reversible and activation control [34].



**Figure 4.** The electrochemical polymerization scheme of (a) PbCmB, (b) P(bCmB-co-bTP), (c) P(bCmB-co-dbBT), and (d) P(bCmB-co-TF).

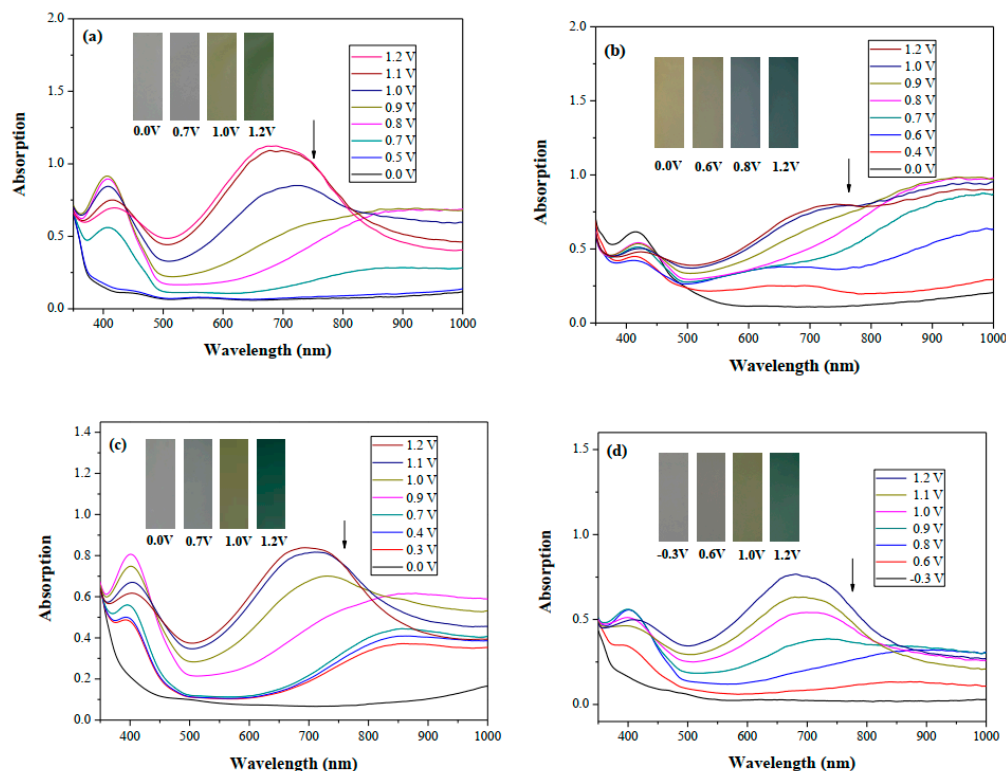


**Figure 5.** (a) CV curves of the P(bCmB-co-bTP) film at scan rates between 10 and 200  $\text{mV s}^{-1}$  in ACN/DCM (1:1 by volume) containing 0.2 M  $\text{LiClO}_4$ . (b) Scan rate dependence of anodic and cathodic peak current densities for the P(bCmB-co-bTP) film.

### 3.2. Absorption Spectra and the Transmittance Changes of the Polymers

Figure 6a–d shows the absorption spectra of the PbCmB, P(bCmB-co-bTP), P(bCmB-co-dbBT), and P(bCmB-co-TF) electrodes in 0.2 M  $\text{LiClO}_4/\text{ACN}/\text{DCM}$ . There was no noticeable absorption peak of the PbCmB film between 370 and 1000 nm at 0.0 and 0.5 V, respectively. As the voltage increased stepwise from 0.0 V to 1.2 V, new charge carrier bands appeared at around 420 and 675 nm, signifying the existence of the generation of radical cations and dication [35] (Figure 6a). As displayed in Figure 6b, P(bCmB-co-bTP) showed a neutral absorption peak at around 420 nm; this could be attributed to the  $\pi$ - $\pi^*$

(or  $n-\pi^*$ ) transition of the bithiophene heteroaromatic groups. The PbCmB film displayed four types of color variations from the neutral to the oxidation state, which were bright gray, dark gray, dark khaki, and dark olive green at 0.0, 0.7, 1.0, and 1.2 V, respectively. The  $L^*$ ,  $a^*$ , and  $b^*$  values of PbCmB are displayed in Table 2. Under identical situations, the P(bCmB-co-bTP) film was celadon, earth gray, iron gray, and navy blue at 0.0, 0.6, 0.8, and 1.2 V, respectively.



**Figure 6.** UV-Vis spectra of (a) PbCmB, (b) P(bCmB-co-bTP), (c) P(bCmB-co-dBBT), and (d) P(bCmB-co-TF) in an ACN/DCM (1:1 by volume) solution containing 0.2 M LiClO<sub>4</sub>.

**Table 2.** Colorimetric values ( $L^*$ ,  $a^*$ , and  $b^*$ ), CIE chromaticity values ( $x$ ,  $y$ ), and diagrams of (a) PbCmB, (b) P(bCmB-co-bTP), (c) P(bCmB-co-dBBT), and (d) P(bCmB-co-TF) at different potentials.

Potential (V)	$L^*$	$a^*$	$b^*$	$x$	$y$	Diagram
(a)						
0.0	91.76	−7.56	9.74	0.319	0.353	
0.7	87.42	−16.01	32.11	0.347	0.407	
0.9	75.15	−25.42	19.31	0.309	0.398	
1.0	64.88	−28.71	7.611	0.277	0.377	
1.2	61.98	−25.31	2.478	0.271	0.359	
(b)						
0.0	87.33	−5.54	32.78	0.365	0.399	
0.4	81.32	−8.09	13.47	0.326	0.364	
0.7	74.83	−11.79	9.61	0.313	0.361	
0.9	70.63	−13.91	6.46	0.303	0.357	
1.2	67.53	−12.56	0.104	0.291	0.340	

Table 2. Cont.

Potential (V)	L*	a*	b*	x	y	Diagram
(c)						
0.0	92.86	−0.44	5.13	0.321	0.339	
0.5	90.67	−6.87	12.66	0.326	0.359	
0.9	80.32	−16.51	20.19	0.326	0.388	
1.0	72.65	−21.29	10.64	0.299	0.373	
1.2	64.68	−21.34	0.542	0.274	0.349	
(d)						
0.0	97.08	−2.03	8.37	0.324	0.345	
0.6	93.67	−4.99	14.82	0.332	0.361	
0.9	82.78	−14.03	14.19	0.318	0.371	
1.1	71.73	−16.35	0.11	0.285	0.342	
1.2	66.68	−18.55	−2.18	0.274	0.339	

The P(bCmB-co-dbBT) film was bright gray, slate gray, khaki, and dark greenish grey at 0.0, 0.7, 1.0, and 1.2 V, respectively. The P(bCmB-co-TF) film was light gray, slate gray, dark khaki, and dark greenish grey at −0.3, 0.6, 1.0, and 1.2 V, respectively. The incorporation of bithiophene, 3,3'-dibromo-2,2'-bithiophene, and 2-(thiophen-2-yl)furan in the polymer chain changed the color variations from the reduced state to the oxidized state.

The optical energy gap ( $E_g$ ) of PbCmB calculated using the absorption onset wavelength ( $\lambda_{\text{onset}}$ ) of the  $\pi$ - $\pi^*$  transition peak was 3.20 eV [36]. Table 3 shows the  $E_g$  of the reported polymers. PbCmB displayed a larger  $E_g$  than PBCPO [37], PMCP [38], and PDCP [39]. This could be attributed to two methylene groups interrupting the conjugated degree of the polymer chains. The  $E_{\text{onset}}$  of PbCmB (vs. Ag/AgNO<sub>3</sub>) was 0.80 V, the  $E_{\text{FOC}}$  calculated from the potential of ferrocene/ferrocenium vs. Ag/AgNO<sub>3</sub> was 0.69 V, and the  $E_{\text{onset}}$  (vs.  $E_{\text{FOC}}$ ) was evaluated as 0.11 V. The reference energy for ferrocene is 4.8 eV below the vacuum level [40].  $E_{\text{HOMO}}$  and  $E_{\text{LUMO}}$ , corresponding with the energy levels of HOMO and LUMO, were calculated as −4.91 and −1.71 eV, respectively.

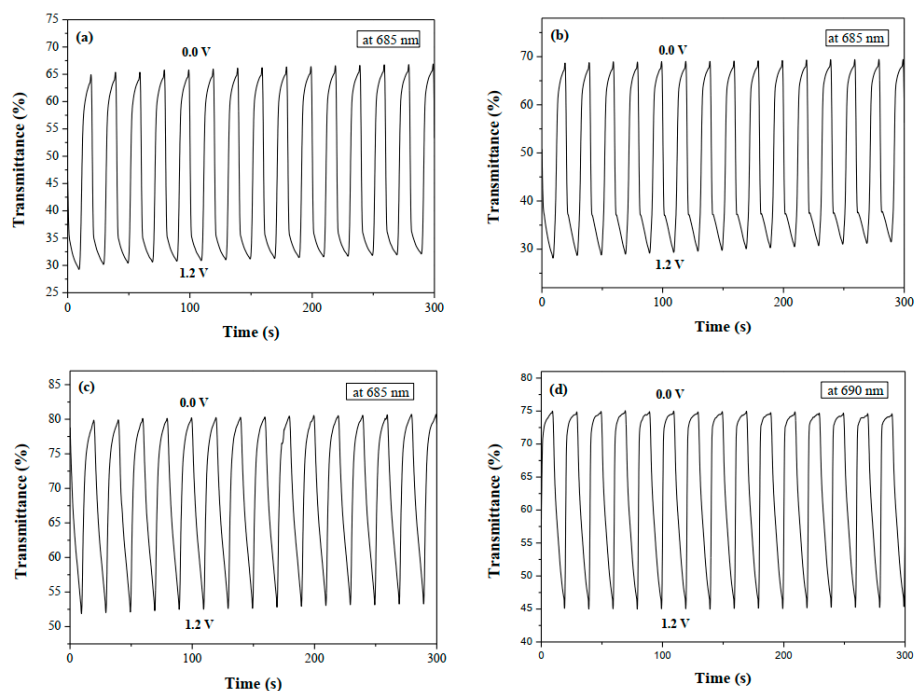
Table 3. Transmittance changes and coloration efficiencies of polymers (or ECDs).

Polymers or ECDs	$\Delta T_{\text{max}}$ (%)	$\eta_{\text{max}}$ (cm <sup>2</sup> ·C <sup>−1</sup> )	$E_g^a$ (eV)	Ref.
PBCPO	30.1 (735nm)	85 (735 nm)	3.14	[37]
PMCP	29 (460 nm)	-	3.14	[38]
PDCP	19 (1025 nm)	124 (1025 nm)	2.58	[39]
PDTCZ-2	30.7 (898 nm)	169 (898 nm)	-	[41]
P(DTC-co-BTP2)	68.4 (855 nm)	159.4 (855 nm)	-	[42]
PbCmB	23.94 (685 nm)	80.3 (685 nm)	3.20	This work
P(bCmB-co-bTP)	39.56 (685 nm)	160.5 (685 nm)	-	This work
PtCz/PProDOT-Me <sub>2</sub>	36 (572 nm)	343.4 (572 nm)	-	[43]
P(Bmco)/PEDOT	35 (620 nm)	-	-	[44]
P(dcbp-co-cpdt)/PEDOT	39.8 (628 nm)	319.98 (628 nm)	-	[45]
P(TTPA-co-EDOT)/PEDOT	20 (775 nm)	336 (775 nm)	-	[46]
P(BCz-co-In)/PProDOT-Et <sub>2</sub>	42.0 (587 nm)	634 (587 nm)	-	[47]
P(DiCP-co-CDTK)/PEDOT-PSS	38 (635 nm)	634 (635 nm)	-	[39]
P(bCmB-co-bTP)/PEDOT	40.7 (635 nm)	428.4 (635 nm)	-	This work

Figure 7 displays the electrochromic switching profiles of PbCmB, P(bCmB-co-bTP), P(bCmB-co-dbBT), and P(bCmB-co-TF) in the solutions, which changed between 0.0 and 1.2 V with a time interval of 10 s. The transmittance changes ( $\Delta T$ ) of PbCmB, P(bCmB-



*co*-bTP), P(bCmB-*co*-dbBT), and P(bCmB-*co*-TF) from the neutral state to the oxidized state were determined to be 23.94% at 685 nm, 39.56% at 685 nm, 27.85% at 685 nm, and 29.84% at 690 nm, respectively. P(bCmB-*co*-bTP) revealed the highest  $\Delta T$  among the four electrodes. The copolymers (P(bCmB-*co*-bTP), P(bCmB-*co*-dbBT), and P(bCmB-*co*-TF)) showed a higher  $\Delta T$  than the homopolymer (PbCmB) in the solutions, suggesting that the electrochemical copolymerization of PbCmB with bithiophene, 3,3'-dibromo-2,2'-bithiophene, or 2-(thiophen-2-yl)furan monomer led to an increase in the  $\Delta T$ . P(bCmB-*co*-bTP) displayed a higher  $\Delta T$  than PBCPO [37], PMCP [38], PDCP [39], and PDT CZ-2 [41]. However, the  $\Delta T$  of P(bCmB-*co*-bTP) was smaller than P(DTC-*co*-BTP2) [42].



**Figure 7.** Optical contrast of (a) PbCmB, (b) P(bCmB-*co*-bTP), (c) P(bCmB-*co*-dbBT), and (d) P(bCmB-*co*-TF) in an ACN/DCM (1:1 by volume) solution containing 0.2 M LiClO<sub>4</sub> with a residence time of 10 s.

The response time from the colored to the bleached state ( $\tau_b$ ) and from the bleached to the colored state ( $\tau_c$ ) of PbCmB, P(bCmB-*co*-bTP), P(bCmB-*co*-dbBT), and P(bCmB-*co*-TF) in the solutions is listed in Table 4. The  $\tau_b$  and  $\tau_c$  were determined at 90% of the maximum  $\Delta T$ . The  $\tau_c$  and  $\tau_b$  of the polymeric films were determined to be 1.46–3.51 s and 4.81–5.18 s, respectively.

**Table 4.** Electrochromic switching properties investigated at specific wavelengths for the electrodes.

Electrodes	$\lambda$ (nm) <sup>a</sup>	$T_{ox}$	$T_{red}$	$\Delta T$	$\Delta OD$	$Q_d$ (mC cm <sup>-2</sup> )	$\eta$ (cm <sup>2</sup> ·C <sup>-1</sup> )	$\tau_c$ (s)	$\tau_b$ (s)
PbCmB	685	71.22	95.16	23.94	0.126	2.78	80.3	1.83	5.10
P(bCmB- <i>co</i> -bTP)	685	28.97	68.53	39.56	0.374	4.19	160.5	3.51	4.81
P(bCmB- <i>co</i> -dbBT)	685	52.07	79.92	27.85	0.186	3.88	86.5	2.64	5.05
P(bCmB- <i>co</i> -TF)	690	45.05	74.89	29.84	0.221	3.25	125.8	1.46	5.18

<sup>a</sup> The selected applied wavelength for the electrodes.

As shown in the following equation [48], the  $\Delta OD$  could be determined by a logarithmic calculation of the transmission (%) at the oxidation state and the reduction state:

$$\Delta OD = \log\left(\frac{T_{ox}}{T_{red}}\right) \quad (1)$$

The  $\Delta OD$ s of the PbCmB, P(bCmB-co-bTP), P(bCmB-co-dbBT), and P(bCmB-co-TF) films in the solutions were 0.126 at 685 nm, 0.374 at 685 nm, 0.186 at 685 nm, and 0.221 at 690 nm, respectively. The P(bCmB-co-bTP), P(bCmB-co-dbBT), and P(bCmB-co-TF) films displayed a higher  $\Delta OD$  than the PbCmB film.

The coloration efficiency ( $\eta$ ) could be obtained from the following equation [48]:

$$\eta = \frac{\Delta OD}{Q_d} \quad (2)$$

where  $Q_d$  represents the charge injection/extraction of the electrodes per active area. As listed in Table 4, the  $\eta$  of PbCmB, P(bCmB-co-bTP), P(bCmB-co-dbBT), and P(bCmB-co-TF) was  $80.3 \text{ cm}^2 \cdot \text{C}^{-1}$  at 685 nm,  $160.5 \text{ cm}^2 \cdot \text{C}^{-1}$  at 685 nm,  $86.5 \text{ cm}^2 \cdot \text{C}^{-1}$  at 685 nm, and  $125.8 \text{ cm}^2 \cdot \text{C}^{-1}$  at 690 nm, respectively.


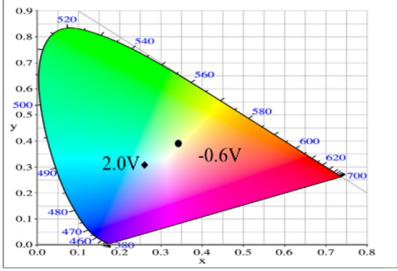




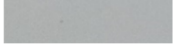
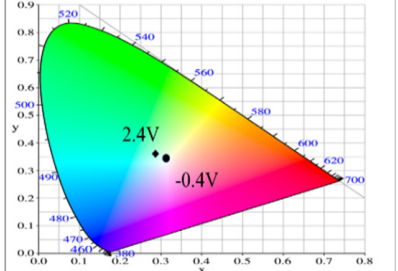
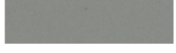
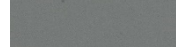
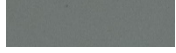


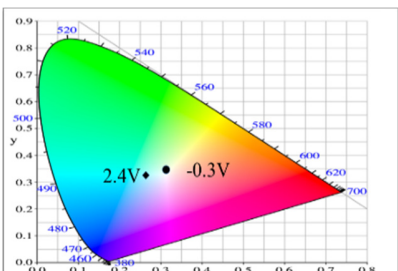




### 3.3. Absorption Spectra and the Transmittance Changes of the ECDs

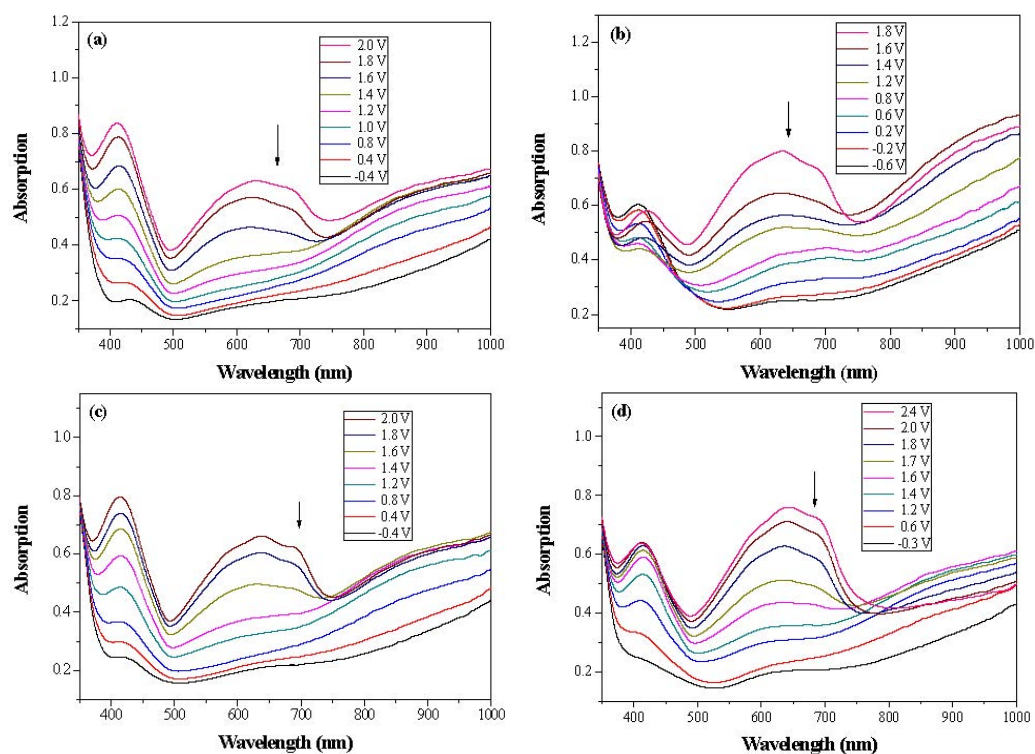
Dual-layer organic ECDs were constructed using the configurations of the PbCmB/PEDOT, P(bCmB-co-bTP)/PEDOT, P(bCmB-co-dbBT)/PEDOT, and P(bCmB-co-TF)/PEDOT ECDs. The absorption spectra of the PbCmB/PEDOT, P(bCmB-co-bTP)/PEDOT, P(bCmB-co-dbBT)/PEDOT, and P(bCmB-co-TF)/PEDOT ECDs are displayed in Figure 8a–d. At  $-0.4 \text{ V}$ , the PbCmB/PEDOT ECD did not reveal a significant absorption peak in the UV-Vis region. The anodic PbCmB film was in its reduced state and the cathodic PEDOT film was in its oxidized state at  $-0.4 \text{ V}$ , exhibiting a limpid color. The PbCmB/PEDOT ECD showed a gainsboro color at  $-0.4 \text{ V}$ . After progressively raising the potential to  $2.0 \text{ V}$ , the PbCmB film started to oxidize and the PEDOT film started to reduce. As a consequence, new absorption bands at  $420$  and  $620 \text{ nm}$  appeared stepwise. The PbCmB/PEDOT ECD showed a dark gray color at  $1.0 \text{ V}$  and a bright slate gray color at  $2.0 \text{ V}$ . Under identical situations, the P(bCmB-co-bTP)/PEDOT ECD was light gray, dark gray, and slate gray at  $-0.6, 0.8,$  and  $2.0 \text{ V}$ , respectively. The P(bCmB-co-dbBT)/PEDOT ECD was gainsboro, dark gray, and bright slate gray at  $-0.4, 1.0,$  and  $2.4 \text{ V}$ , respectively. The P(bCmB-co-TF)/PEDOT ECD was gainsboro, light gray, and dark gray at  $-0.3, 1.6,$  and  $2.4 \text{ V}$ , respectively. The colorimetric results of the four ECDs are listed in Table 5.

**Table 5.** Electrochromic photographs, colorimetric values ( $L^*$ ,  $a^*$ , and  $b^*$ ), CIE chromaticity values ( $x$ ,  $y$ ), and diagrams of (a) PbCmB/PEDOT, (b) P(bCmB-co-bTP)/PEDOT, (c) P(bCmB-co-dbBT)/PEDOT, and (d) P(bCmB-co-TF)/PEDOT ECDs at different potentials.

ECD	Potential (V)	Photographs	$L^*$	$a^*$	$b^*$	$x$	$y$	Diagram
(a)								
PbCmB/PEDOT	$-0.4$		86.69	$-5.91$	2.73	0.309	0.339	
	$0.8$		83.53	$-9.09$	9.36	0.317	0.356	
	$1.0$		81.24	$-10.17$	10.88	0.318	0.361	
	$1.4$		74.73	$-13.07$	12.32	0.317	0.369	
	$2.0$		62.04	$-18.35$	6.08	0.292	0.364	

Table 5. Cont.

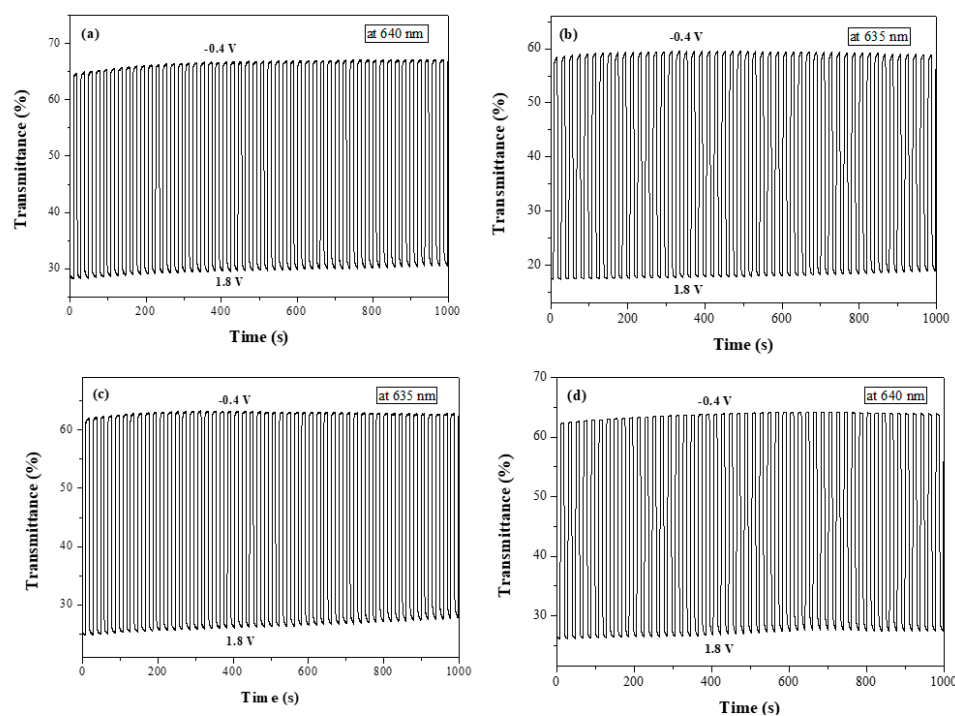
ECD	Potential (V)	Photographs	L*	a*	b*	x	y	Diagram
(b)								
P(bCmB-co-bTP)/PEDOT	−0.6		80.63	−9.79	22.19	0.341	0.386	
	0.2		78.28	−10.98	14.81	0.325	0.371	
	0.8		72.73	−9.73	3.32	0.303	0.345	
	1.2		67.11	−8.04	−4.71	0.288	0.324	
	2.0		54.98	−10.98	−11.85	0.259	0.304	
(c)								
P(bCmB-co-dbBT)/PEDOT	−0.4		85.41	−5.95	3.44	0.311	0.341	
	0.8		82.06	−8.31	8.14	0.316	0.353	
	1.0		73.75	−12.33	10.88	0.315	0.365	
	1.4		68.06	−14.97	7.90	0.304	0.363	
	2.4		61.64	−18.83	3.63	0.285	0.357	
(d)								
P(bCmB-co-TF)/PEDOT	−0.3		86.25	−6.88	4.39	0.311	0.343	
	1.2		78.49	−9.49	7.62	0.313	0.354	
	1.6		68.04	−14.27	3.33	0.295	0.349	
	1.9		63.71	−15.82	−2.15	0.278	0.337	
	2.4		59.47	−16.45	−7.49	0.262	0.322	



**Figure 8.** UV-Vis spectra of (a) PbCmB/PEDOT, (b) P(bCmB-co-bTP)/PEDOT, (c) P(bCmB-co-dbBT)/PEDOT, and (d) P(bCmB-co-TF)/PEDOT ECDs.

Figure 9 shows the color-bleach kinetics of the PbCmB/PEDOT, P(bCmB-co-bTP)/PEDOT, P(bCmB-co-dbBT)/PEDOT, and P(bCmB-co-TF)/PEDOT ECDs; the time interval of the cycle switched between  $-0.4$  V and  $1.8$  V was 10 s. Table 6 lists the  $\Delta T$ ,  $\Delta OD$ ,  $\eta$ ,  $\tau_b$ , and  $\tau_c$  of the four ECDs. The  $\Delta T$  of the PbCmB/PEDOT, P(bCmB-co-bTP)/PEDOT, P(bCmB-co-dbBT)/PEDOT, and P(bCmB-co-TF)/PEDOT ECDs was 35.3% at 640 nm, 40.7% at 635 nm, 36.4% at 635 nm, and 35.7% at 640 nm at the second cycle, respectively. The P(bCmB-co-bTP)/PEDOT ECD showed the highest  $\Delta T$ . The P(bCmB-co-bTP)/PEDOT, P(bCmB-co-dbBT)/PEDOT, and P(bCmB-co-TF)/PEDOT ECDs displayed a higher  $\Delta T$  than the PbCmB/PEDOT ECD, indicating that the use of bithiophene, 3,3'-dibromo-2,2'-bithiophene, and 2-(thiophen-2-yl)furan-containing copolymers as the anodically coloring layers in the ECDs gave rise to a higher  $\Delta T$  than the PbCmB. The P(bCmB-co-bTP)/PEDOT ECD displayed a higher  $\Delta T$  than the PtCz/PProDOT-Me<sub>2</sub> [43], P(Bmco)/PEDOT [44], P(dcbp-co-cpdt)/PEDOT [45], P(DiCP-co-CDTK)/PEDOT-PSS [39], and P(TTPA-co-EDOT)/PEDOT ECDs [46]. However, the P(bCmB-co-bTP)/PEDOT ECD showed a lower  $\Delta T$  than the P(BCz-co-In)/PProDOT-Et<sub>2</sub> ECD [47].

The  $\eta$  of the dual-layer organic ECDs is also shown in Table 6. The  $\eta$  of the PbCmB/PEDOT, P(bCmB-co-bTP)/PEDOT, P(bCmB-co-dbBT)/PEDOT, and P(bCmB-co-TF)/PEDOT ECDs was  $305.8 \text{ cm}^2 \cdot \text{C}^{-1}$  at 640 nm,  $428.4 \text{ cm}^2 \cdot \text{C}^{-1}$  at 635 nm,  $341.0 \text{ cm}^2 \cdot \text{C}^{-1}$  at 635 nm, and  $316.8 \text{ cm}^2 \cdot \text{C}^{-1}$  at 640 nm at the second cycle, respectively. The P(bCmB-co-bTP)/PEDOT ECD displayed the highest  $\eta$ . The use of P(bCmB-co-bTP), P(bCmB-co-dbBT), and P(bCmB-co-TF) as the anodically coloring materials in the ECDs led to a higher  $\eta$  than the PbCmB. Table 3 also summarizes the  $\eta$  of the reported ECDs. The P(bCmB-co-bTP)/PEDOT ECD showed a higher  $\eta$  than the PtCz/PProDOT-Me<sub>2</sub> [43], P(dcbp-co-cpdt)/PEDOT [45], and P(TTPA-co-EDOT)/PEDOT ECDs [46]. However, the P(bCmB-co-bTP)/PEDOT ECD displayed a lower  $\eta$  than the P(BCz-co-In)/PProDOT-Et<sub>2</sub> [47] and P(DiCP-co-CDTK)/PEDOT-PSS ECDs [39].



**Figure 9.** Optical contrast of (a) PbCmB/PEDOT, (b) P(bCmB-co-bTP)/PEDOT, (c) P(bCmB-co-dbBT)/PEDOT, and (d) P(bCmB-co-TF)/PEDOT ECDs with a residence time of 10 s.

**Table 6.** Electrochromic switching properties investigated at specific wavelengths for four devices.

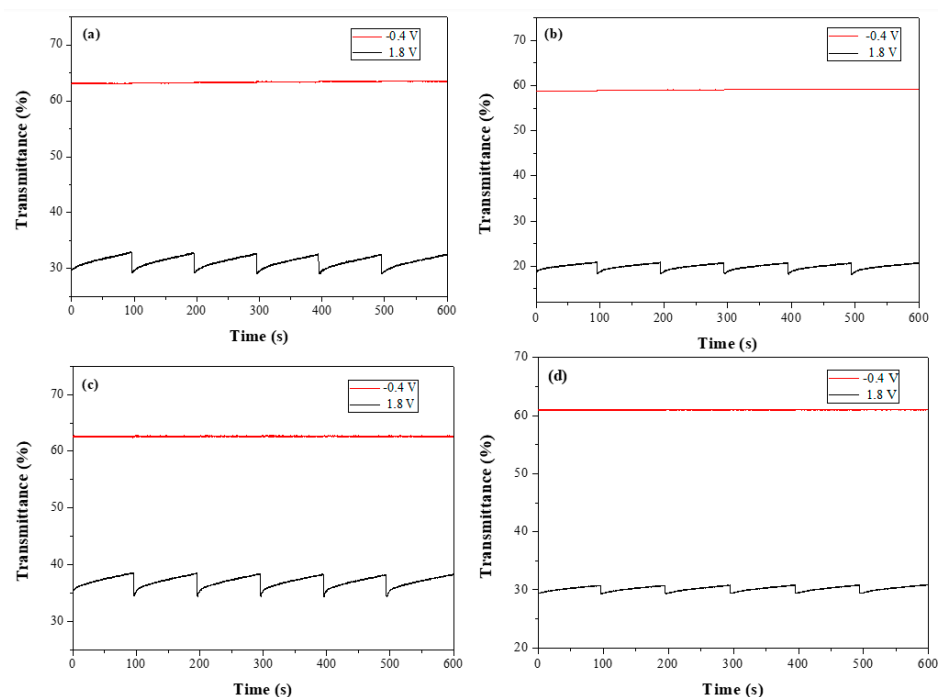
ECDs	$\lambda$ (nm)	$N$	$T_{ox}$	$T_{red}$	$\Delta T$	$\Delta OD$	$Q_d$ (mC cm <sup>-2</sup> )	$\eta$ (cm <sup>2</sup> ·C <sup>-1</sup> )	$\tau_c$ (s)	$\tau_b$ (s)
PbCmB/PEDOT	640	2	29.5	64.8	35.3	0.341	1.45	305.8	1.8	1.8
		60	34.1	67.2	33.1	0.295	1.33	288.3	1.8	1.9
P(bCmB-co-bTP)/PEDOT	635	2	18.0	58.7	40.7	0.514	1.56	428.4	1.9	1.8
		60	20.9	58.4	37.5	0.447	1.47	395.3	1.9	2.5
P(bCmB-co-dbBT)/PEDOT	635	2	25.7	62.1	36.4	0.383	1.46	341.0	1.8	1.9
		60	28.7	62.6	33.9	0.339	1.32	333.8	1.8	2.8
P(bCmB-co-TF)/PEDOT	640	2	26.8	62.5	35.7	0.368	1.51	316.8	1.9	1.9
		60	28.9	63.6	34.7	0.342	1.46	304.5	1.8	1.6

The response time of the PbCmB/PEDOT, P(bCmB-co-bTP)/PEDOT, P(bCmB-co-dbBT)/PEDOT, and P(bCmB-co-TF)/PEDOT ECDs was shorter than the PbCmB, P(bCmB-co-bTP), P(bCmB-co-dbBT), and P(bCmB-co-TF) electrodes in the solutions, disclosing that the distances between the anode and the cathode in the ECDs were narrower than between the polymeric electrode and the Pt electrode in the solutions [49].

### 3.4. Open Circuit Memories of the ECDs

The open circuit memories of the dual-layer organic ECDs were monitored by applying potentials in colored and bleached states for 1 s for each 100 s interval. As displayed in Figure 10, the PbCmB/PEDOT, P(bCmB-co-bTP)/PEDOT, P(bCmB-co-dbBT)/PEDOT, and P(bCmB-co-TF)/PEDOT ECDs displayed sufficient open circuit memories with  $\leq 1.1\%$  transmittance variation in the bleached state. However, in an oxidized state of the PbCmB, P(bCmB-co-bTP), P(bCmB-co-dbBT), and P(bCmB-co-TF) films and in a reduced state of the PEDOT film, the transmittance changes of the PbCmB/PEDOT, P(bCmB-co-bTP)/PEDOT, P(bCmB-co-dbBT)/PEDOT, and P(bCmB-co-TF)/PEDOT ECDs in a colored state were less

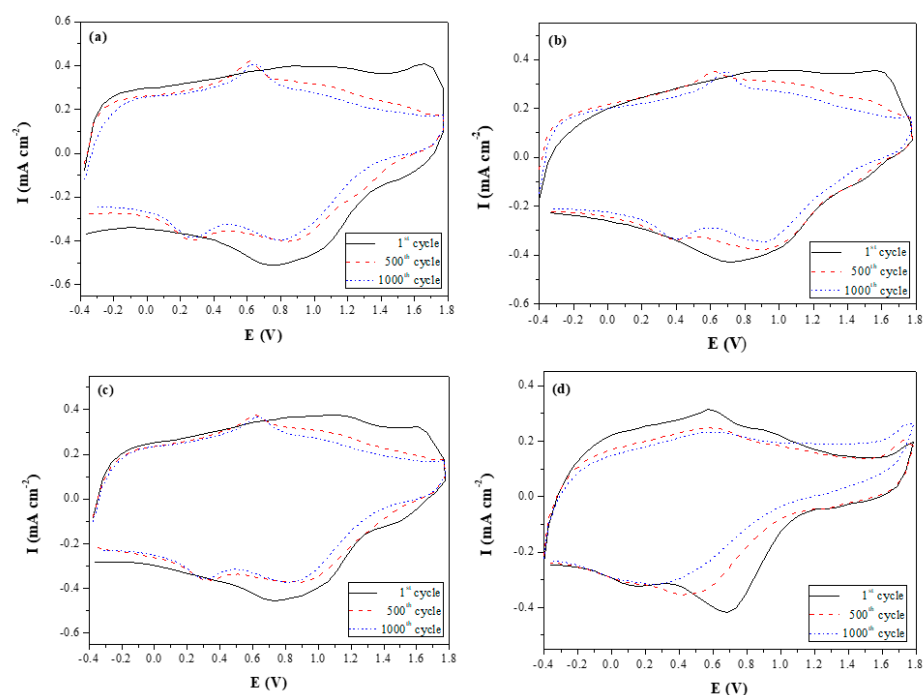
stable than the four ECDs in a bleached state. The P(bCmB-co-dbBT)/PEDOT ECD showed the largest transmittance change in a colored state. However, the transmittance change of the P(bCmB-co-dbBT)/PEDOT ECD in a colored state was less than 4.9%, implying that the PbCmB/PEDOT, P(bCmB-co-bTP)/PEDOT, P(bCmB-co-dbBT)/PEDOT, and P(bCmB-co-TF)/PEDOT ECDs had ample open circuit memories in both the colored and bleached states.



**Figure 10.** Open circuit stability of the (a) PbCmB/PEDOT, (b) P(bCmB-co-bTP)/PEDOT, (c) P(bCmB-co-dbBT)/PEDOT, and (d) P(bCmB-co-TF)/PEDOT ECDs.

### 3.5. Long-Term Electrochemical Redox Stability of the ECDs

The long-term cyclic voltammetry stability of the PbCmB/PEDOT, P(bCmB-co-bTP)/PEDOT, P(bCmB-co-dbBT)/PEDOT, and P(bCmB-co-TF)/PEDOT ECDs was detected for 1000th cycles with a scan speed of  $500 \text{ mV}\cdot\text{s}^{-1}$ . As displayed in Figure 11, 84.9%, 92.8%, 85.4%, and 85.7% of the electrochemical activity was maintained at the 500th cycle, respectively, and 75.5%, 81.5%, 78.2%, and 76.6% of the electrochemical activity was maintained at the 1000th cycle for the PbCmB/PEDOT, P(bCmB-co-bTP)/PEDOT, P(bCmB-co-dbBT)/PEDOT, and P(bCmB-co-TF)/PEDOT ECDs, respectively. The P(bCmB-co-bTP)/PEDOT, P(bCmB-co-dbBT)/PEDOT, and P(bCmB-co-TF)/PEDOT ECDs that used copolymers as anodic layers showed a better long-term stability than the PbCmB/PEDOT ECD at the 500th and 1000th cycles.



**Figure 11.** Cyclic voltammograms of (a) PbCmB/PEDOT, (b) P(bCmB-co-bTP)/PEDOT, (c) P(bCmB-co-dbBT)/PEDOT, and (d) P(bCmB-co-TF)/PEDOT ECDs as a function of repeated cycles with a scan rate of  $500 \text{ mV s}^{-1}$  between 1 and 1000 cycles.

#### 4. Conclusions

A series of redox-active polycarbazoles (PbCmB, P(bCmB-co-bTP), P(bCmB-co-dbBT), and P(bCmB-co-TF)) were electrochemically synthesized onto ITO glass surfaces. The obtained polycarbazoles showed a good redox reversibility. Compared with the homopolymer, the copolymers showed different color transitions from the neutral to the oxidized states. The P(bCmB-co-bTP) film was celadon, earth gray, iron gray, and navy blue at 0.0, 0.6, 0.8, and 1.2 V, respectively. Electrochromic switching studies of the four polycarbazoles exhibited that the  $\Delta T$  of PbCmB and P(bCmB-co-TF) was 23.94% at 685 nm and 29.84% at 690 nm, respectively. Four ECDs were built using anodic polycarbazoles and a cathodic PEDOT layer. The  $\Delta T$  of the PbCmB/PEDOT and P(bCmB-co-dbBT)/PEDOT ECDs was 35.3% at 640 nm and 36.4% at 635 nm at the second cycle, respectively. bCmB-containing polycarbazoles and their corresponding ECDs showed high transmittance changes. The incorporation of bithiophene, 3,3'-dibromo-2,2'-bithiophene, and 2-(thiophen-2-yl)furan groups into the polycarbazoles showed different color transitions at various potentials and showed high transmittance changes. Moreover, five ECDs displayed a fast response time ( $\leq 2.8 \text{ s}$ ) and satisfactory open circuit memories in both the colored and bleached states. As a result, PbCmB and P(bCmB-co-bTP) may be good candidates for use as electrodes in ECDs.

**Author Contributions:** C.-W.K. conceived the research topic. Y.-D.L. and T.-Y.W. carried out the experiments. C.-W.K., T.-Y.W., J.-C.C., L.-T.L. and P.-Y.L. analyzed the electrochromic properties. All authors have read and agreed to the published version of the manuscript.

**Funding:** This research was funded by the Ministry of Science and Technology of the Republic of China, Grant No. 110-2221-E-992-051 and 108-2221-E-224-049-MY3.

**Conflicts of Interest:** The authors declare no conflict of interest.

## References

1. Mortimer, R.J. Electrochromic materials. *Annu. Rev. Mater. Res.* **2011**, *41*, 241–268. [[CrossRef](#)]
2. Wu, W.; Wang, M.; Ma, J.; Cao, Y.; Deng, Y. Electrochromic metal oxides: Recent progress and prospect. *Adv. Electron. Mater.* **2018**, *4*, 1800185. [[CrossRef](#)]
3. Mortimer, R.J.; Dyer, A.L.; Reynolds, J.R. Electrochromic organic and polymeric materials for display applications. *Displays* **2006**, *27*, 12–18. [[CrossRef](#)]
4. Rai, V.; Singh, R.S.; Blackwood, D.J.; Zhili, D. A review on recent advances in electrochromic devices: A material approach. *Adv. Eng. Mater.* **2020**, *22*, 2000082. [[CrossRef](#)]
5. Shah, K.W.; Wang, S.-X.; Soo, D.X.Y.; Xu, J. Viologen-based electrochromic materials: From small molecules, polymers and composites to their applications. *Polymers* **2019**, *11*, 1839. [[CrossRef](#)]
6. Ditte, K.; Kiriy, N.; Perez, J.; Hamsch, M.; Mannsfeld, S.C.B.; Krupskaya, Y.; Maragani, R.; Voit, B.; Lissel, F. Charge carrier mobility improvement in diketopyrrolopyrrole block-copolymers by shear coating. *Polymers* **2021**, *13*, 1435. [[CrossRef](#)]
7. Jeong, M.K.; Suh, E.H.; Lee, K.; Jang, J.; Jung, I.H. Acceptor-acceptor-type conjugated polymer for use in n-type organic thin-film transistors and thermoelectric devices. *Org. Electron.* **2020**, *86*, 105921. [[CrossRef](#)]
8. Kuo, C.W.; Chang, J.C.; Wu, B.W.; Wu, T.Y. Electrochemical characterization of RuO<sub>2</sub>-Ta<sub>2</sub>O<sub>5</sub>/polyaniline composites as potential redox electrodes for super-capacitor and hydrogen evolution reaction. *Int. J. Hydrogen Energy* **2020**, *45*, 22223–22231. [[CrossRef](#)]
9. Fu, W.C.; Hsieh, Y.T.; Wu, T.Y.; Sun, I.W. Electrochemical preparation of porous poly(3,4-ethylenedioxythiophene) electrodes from room temperature ionic liquids for supercapacitors. *J. Electrochem. Soc.* **2016**, *163*, G61–G68. [[CrossRef](#)]
10. Mkawi, E.M.; Al-Hadeethi, Y.; Bazuhair, R.S.; Yousef, A.S.; Shalaan, E.; Arkook, B.; Abdeldaiem, A.M.; Almalki, R.; Bekyarova, E. Optimization of Sb<sub>2</sub>S<sub>3</sub> nanocrystal concentrations in P<sub>3</sub>HT: PCBM layers to improve the performance of polymer solar cells. *Polymers* **2021**, *13*, 2152. [[CrossRef](#)]
11. Lanzi, M.; Quadretti, D.; Marinelli, M.; Ziai, Y.; Salatelli, E.; Pierini, F. Influence of the active layer structure on the photovoltaic performance of water-soluble polythiophene-based solar cells. *Polymers* **2021**, *13*, 1640. [[CrossRef](#)] [[PubMed](#)]
12. Wu, T.Y.; Lee, N.C.; Chen, Y. Synthesis and characterization of new poly(pphenylenevinylene) derivative containing 5,5'-diphenyl-2,2'-p-(2,5-bis(hexyloxy)phenylene)bis-1,3,4-oxadiazole and distyrylbenzene moieties. *Synth. Met.* **2003**, *139*, 263–269. [[CrossRef](#)]
13. Liu, Q.; Moghe, D.; Sardar, G.; Manzhos, S.; Bottle, S.E.; Kyaw, A.K.K.; Kabra, D.; Sonar, P. Structural geometry variation of 1,4-naphthalene-based co-polymers to tune the device performance of PVK-host-based OLEDs. *Polymers* **2021**, *13*, 2914. [[CrossRef](#)] [[PubMed](#)]
14. Dinesh, G.K.; Chakma, S. Degradation kinetic study of cholesterol lowering statin drug-using sono-hybrid techniques initiated by metal-free polymeric catalyst. *J. Taiwan Inst. Chem. Eng.* **2019**, *100*, 95–104. [[CrossRef](#)]
15. Kuo, C.W.; Lu, C.W.; Chang, J.K.; Chen, H.R.; Wu, T.Y. Composites of platinum particles embedded into poly(6-cyanoindole)/poly(styrenesulfonic acid) for methanol oxidation. *Int. J. Hydrogen Energy* **2021**, *46*, 16644–16654. [[CrossRef](#)]
16. Boali, A.A.; Mansha, M.; Waheed, A.; Ullah, N. Synthesis and selective colorimetric detection of iodide ion by novel 1,5-naphthyridine-based conjugated polymers. *J. Taiwan Inst. Chem. Eng.* **2018**, *91*, 420–426. [[CrossRef](#)]
17. Wu, T.Y.; Sheu, R.B.; Chen, Y. Synthesis and optically acid-sensory and electrochemical properties of novel polyoxadiazole derivatives. *Macromolecules* **2004**, *37*, 725–733. [[CrossRef](#)]
18. An, L.; Tong, J.; Huang, Y.; Liang, Z.; Li, J.; Yang, C.; Wang, X. Elevated photovoltaic performance in medium bandgap copolymers composed of indacenodi-thieno[3,2-b]thiophene and benzothiadiazole subunits by modulating the  $\pi$ -bridge. *Polymers* **2020**, *12*, 368. [[CrossRef](#)]
19. Firda, P.B.D.; Malik, Y.T.; Oh, J.K.; Wujcik, E.K.; Jeon, J.-W. Enhanced chemical and electrochemical stability of polyaniline-based layer-by-layer films. *Polymers* **2021**, *13*, 2992. [[CrossRef](#)]
20. Popov, A.; Brasiunas, B.; Damaskaite, A.; Plikusiene, I.; Ramanavicius, A.; Ramanaviciene, A. Electrodeposited gold nanostructures for the enhancement of electrochromic properties of PANI-PEDOT film deposited on transparent electrode. *Polymers* **2020**, *12*, 2778. [[CrossRef](#)]
21. Kuo, C.W.; Wu, T.Y.; Fan, S.C. Applications of poly(indole-6-carboxylic acid-co-2,2'-bithiophene) films in high-contrast electrochromic devices. *Coatings* **2018**, *8*, 102. [[CrossRef](#)]
22. Jiang, M.; Sun, Y.; Ning, J.; Chen, Y.; Wu, Y.; Hu, Z.; Shuja, A.; Meng, H. Diphenyl sulfone based multicolored cathodically coloring electrochromic materials with high contrast. *Org. Electron.* **2020**, *83*, 105741. [[CrossRef](#)]
23. Zhang, Y.; Chen, S.; Zhang, Y.; Du, H.; Zhao, J. Design and characterization of new D-A type electrochromic conjugated copolymers based on indolo[3,2-b]carbazole, isoindigo and thiophene units. *Polymers* **2019**, *11*, 1626. [[CrossRef](#)] [[PubMed](#)]
24. Karabay, L.C.; Karabay, B.; Karakoy, M.S.; Cihaner, A. Effect of furan, thiophene and selenophene donor groups on benzoselenadiazole based donor-acceptor-donor systems. *J. Electroanal. Chem.* **2016**, *780*, 84–89. [[CrossRef](#)]
25. Hsiao, S.H.; Huang, Y.P. Redox-active and fluorescent pyrene-based triarylamine dyes and their derived electrochromic polymers. *Dye. Pigm.* **2018**, *158*, 368–381. [[CrossRef](#)]
26. Kuo, C.W.; Chen, B.K.; Li, W.B.; Tseng, L.Y.; Wu, T.Y.; Tseng, C.G.; Chen, H.R.; Huang, Y.C. Effects of supporting electrolytes on spectroelectrochemical and electrochromic properties of polyaniline-poly(styrene sulfonic acid) and poly(ethylenedioxythiophene)-poly(styrene sulfonic acid)-based electrochromic device. *J. Chin. Chem. Soc.* **2014**, *61*, 563–570. [[CrossRef](#)]



27. Soganci, T.; Baygu, Y.; Gök, Y.; Ak, M. Disulfide-linked symmetric *N*-alkyl carbazole derivative as a new electroactive monomer for electrochromic applications. *Synth. Met.* **2018**, *244*, 120–127. [[CrossRef](#)]
28. Zheng, R.; Huang, T.; Zhang, Z.; Sun, Z.; Niu, H.; Wang, C.; Wang, W. Novel polyimides containing flexible carbazole blocks with electrochromic and electrofluorescencechromic properties. *RSC Adv.* **2020**, *10*, 6992–7003. [[CrossRef](#)]
29. Tung, T.S.; Ho, K.C. Cycling and at-rest stabilities of a complementary electrochromic device containing poly(3,4-ethylenedioxythiophene) and prussian blue. *Sol. Energy Mater. Sol. Cells* **2006**, *90*, 521–537. [[CrossRef](#)]
30. Roncali, J.; Lemaire, M.; Garreau, R.; Garnier, F. Proceedings of the international conference of science and technology of synthetic metals enhancement of the mean conjugation length in conducting polythiophenes. *Synth. Met.* **1987**, *18*, 139–144. [[CrossRef](#)]
31. Guzel, M.; Karatas, E.; Ak, M. Multifunctional surface design by carbazole and fluorescein functionalized conducting polymer: High-contrast electrochromic devices application. *J. Electrochem. Soc.* **2018**, *165*, 437–445. [[CrossRef](#)]
32. Kuo, C.W.; Chang, J.C.; Huang, W.C.; Lee, P.Y.; Wu, T.Y. Electrochromic polymers based on 2,5-di(thiophen-2-yl)thieno[3,2-b]thiophene and thiophene derivatives as potential anodic layers for high performance electrochromic devices. *J. Taiwan Inst. Chem. Eng.* **2021**, *125*, 41–57. [[CrossRef](#)]
33. Hsiao, S.H.; Lin, S.W. Electrochemical synthesis of electrochromic polycarbazole films from *N*-phenyl-3,6-bis(*N*-carbazolyl)carbazoles. *Polym. Chem.* **2016**, *7*, 198–211. [[CrossRef](#)]
34. Wang, W.-H.; Chang, J.-C.; Lee, P.-Y.; Lin, Y.-C.; Wu, T.-Y. 4-(Trifluoromethoxy)phenyl-containing polymers as promising anodic materials for electrochromic devices. *Coatings* **2020**, *10*, 1251. [[CrossRef](#)]
35. Zhang, Y.; Liu, F.; Hou, Y.; Niu, H. Soluble high coloration efficiency electrochromic polymers based on (*N*-phenyl)carbazole, triphenylamine and 9,9-dioctyl-9H-fluorene. *Synth. Met.* **2019**, *247*, 81–89. [[CrossRef](#)]
36. Kuo, C.W.; Chang, J.C.; Huang, Y.T.; Chang, J.K.; Lee, L.T.; Wu, T.Y. Applications of copolymers consisting of 2,6-di(9H-carbazol-9-yl)pyridine and 3,6-di(2-thienyl)carbazole units as electrodes in electrochromic devices. *Materials* **2019**, *12*, 1251. [[CrossRef](#)]
37. Kuo, C.W.; Chang, J.C.; Lee, L.T.; Chang, J.K.; Huang, Y.T.; Lee, P.Y.; Wu, T.Y. Electrosynthesis of electrochromic polymers based on bis-(4-(*N*-carbazolyl)phenyl)-phenylphosphine oxide and 3,4-propylenedioxythiophene derivatives and studies of their applications in high contrast dual type electrochromic devices. *J. Taiwan Inst. Chem. Eng.* **2022**, *131*, 104173. [[CrossRef](#)]
38. Wang, B.; Zhao, J.; Xiao, J.; Cui, C.; Liu, R. Synthesis and electropolymerization of 9H-carbazol-9-ylpyrene and its electrochromic properties and electrochromic device application. *Int. J. Electrochem. Sci.* **2012**, *7*, 2781–2795.
39. Kuo, C.W.; Wu, B.W.; Chang, J.K.; Chang, J.C.; Lee, L.T.; Wu, T.Y.; Ho, T.H. Electrochromic devices based on poly(2,6-di(9H-carbazol-9-yl)pyridine)-type polymer films and PEDOT-PSS. *Polymers* **2018**, *10*, 604. [[CrossRef](#)]
40. Su, Y.S.; Chang, J.C.; Wu, T.Y. Applications of three dithienylpyrroles-based electrochromic polymers in high-contrast electrochromic devices. *Polymers* **2017**, *9*, 114. [[CrossRef](#)]
41. Zhang, Y.; Kong, L.; Ju, X.; Du, H.; Zhao, J.; Xie, Y. Synthesis and characterization of novel donor–acceptor type neutral green electrochromic polymers containing an indolo[3,2-b]carbazole donor and diketopyrrolopyrrole acceptor. *RSC Adv.* **2018**, *8*, 21252. [[CrossRef](#)]
42. Kuo, C.W.; Chang, J.C.; Chang, J.K.; Huang, S.W.; Lee, P.Y.; Wu, T.Y. Electrosynthesis of electrochromic polymer membranes based on 3,6-di(2-thienyl)carbazole and thiophene derivatives. *Membranes* **2021**, *11*, 125. [[CrossRef](#)] [[PubMed](#)]
43. Kuo, C.W.; Chang, J.K.; Lin, Y.C.; Wu, T.Y.; Lee, P.Y.; Ho, T.H. Poly(tris(4-carbazoyl-9-ylphenyl)amine)/three poly(3,4-ethylenedioxythiophene) derivatives in complementary high-contrast electrochromic devices. *Polymers* **2017**, *9*, 543. [[CrossRef](#)] [[PubMed](#)]
44. Koyuncu, S.; Gultekin, B.; Zafer, C.; Bilgili, H.; Can, M.; Demic, S.; Kaya, I.; Icli, S. Electrochemical and optical properties of biphenyl bridged-dicarbazole oligomer films: Electropolymerization and electrochromism. *Electrochim. Acta* **2009**, *54*, 5694–5702. [[CrossRef](#)]
45. Chen, S.; Gao, Q.; Zhao, J.; Cui, C.; Yang, W.; Zhang, X. Electrosynthesis, characterizations and electrochromic properties of a novel copolymer of 4,4'-di(*N*-carbazoyl)biphenyl with 4H-cyclopenta[2,1-b:3,4-b']dithiophene. *Int. J. Electrochem. Sci.* **2012**, *7*, 5256–5272.
46. Cheng, X.; Zhao, J.; Fu, Y.; Cui, C.; Zhang, X. Electrosynthesis and characterization of a multielectrochromic copolymer of tris[4-(2-thienyl)phenyl]amine with 3,4-ethylenedioxythiophene. *J. Electrochem. Soc.* **2019**, *160*, G6–G13. [[CrossRef](#)]
47. Kuo, C.W.; Wu, T.Y.; Huang, M.W. Electrochromic characterizations of copolymers based on 4,4-bis(*N*-carbazolyl)-1,1-biphenyl and indole-6-carboxylic acid and their applications in electrochromic devices. *J. Taiwan Inst. Chem. Eng.* **2016**, *6*, 481–488. [[CrossRef](#)]
48. Wu, T.Y.; Tung, Y.H. Phenylthiophene-containing poly(2,5-dithienylpyrrole)s as potential anodic layers for high-contrast electrochromic devices. *J. Electrochem. Soc.* **2018**, *165*, H183–H195. [[CrossRef](#)]
49. Kuo, C.W.; Chang, J.C.; Chang, J.K.; Huang, S.W.; Lee, P.Y.; Wu, T.Y. Electrodeposited copolymers based on 9,9'-(5-bromo-1,3-phenylene)biscarbazole and dithiophene derivatives for high-performance electrochromic devices. *Polymers* **2021**, *13*, 1136. [[CrossRef](#)]